Accepted Manuscript

The structural and electronic properties of Pt-Cu alloy clusters: Embedding atom method combined with density functional theory study

Xueling Lei, Haimen Mu, Shuai Li, Gang Liu, Bo Xu, Chuying Ouyang

PII: S0925-8388(18)30151-8

DOI: 10.1016/j.jallcom.2018.01.150

Reference: JALCOM 44614

To appear in: *Journal of Alloys and Compounds*

Received Date: 18 October 2017

Revised Date: 8 January 2018

Accepted Date: 10 January 2018

Please cite this article as: X. Lei, H. Mu, S. Li, G. Liu, B. Xu, C. Ouyang, The structural and electronic properties of Pt-Cu alloy clusters: Embedding atom method combined with density functional theory study, *Journal of Alloys and Compounds* (2018), doi: 10.1016/j.jallcom.2018.01.150.

The structural and electronic properties of Pt-Cu alloy clusters: embedding atom method combined with density functional theory study

Xueling Lei[1], Haimen Mu, Shuai Li, Gang Liu, Bo Xu, Chuying Ouyang

Department of Physics, Laboratory of Computational Materials Physics, Jiangxi Normal University, Nanchang, Jiangxi 330022, China

Abstract: Using an embedding atom method, the low-lying candidate structures of a large Pt-Cu alloy cluster $Pt_{86}Cu_{22}$ were obtained through screening 10^5 isomers. The results indicate that the Pt@PtCu core-shell structures with Pt skin and PtCu core are energetically more stable than the others, which is in good agreement with the experimental observation. Furthermore, an impurity Cu atom is preferred to stay at the subsurface instead of the surface region of Pt-Cu alloy clusters, and the doped Cu atoms prefer to disperse in Pt-Cu alloy. The electronic structures of the EAM optimized structures are calculated with density functional theory, and the projected electronic densities of states reveal that Cu doping can obviously enrich the electronic states of surface Pt atoms near the Fermi level, which may provide some clues for understanding the mechanism of enhancement of the catalytic activity for Pt-Cu alloy catalyst.

Keywords: Pt-Cu alloy clusters; embedding atom method; first-principles calculations; geometry structures; electronic properties

[1]Corresponding author: Xueling Lei, xueling@mail.ustc.edu.cn

1. Introduction

In the past decades, proton exchange membrane fuel cells (PEMFCs) have attracted much attention due to their unique properties such as low operating temperature, low environmental pollution, and relatively high energy density [1].They are expected to be widely used in electric vehicles (EV) as alternative clean power sources. However, the high cost of platinum (Pt) catalysts in PEMFCs has become one of the biggest obstacles to the commercialization of such devices. Recently, it has been found that alloying Pt with cheap transition metals (TM) such as Cu, Ni, Co, Fe, etc., has dual advantages. First, this will reduce the usage of Pt and make the PEMFC technology economically more viable. On the other hand, the Pt-based alloy catalysts have shown higher activity than the Pt itself towards the oxygen reduction reaction (ORR) [2-10]. Among those being reported recently, the Pt-Cu system is the most promising and has received considerable interest due to the largely improved catalytic activity. Using different methods like electrodeposition [11-12], one-pot synthesis method [13], and electrochemical dealloying [14-15], a variety of nano-structures of the Pt-Cu alloy has been achieved. For example, using a composition-controlled electrochemical dealloying method, Chen et al. [14] reported a nanoporous core-shell Pt-Cu catalyst, which has a Pt only skin while Pt-Cu alloy core, which has exhibited a very high catalytic activity towards oxygen reduction reaction and formic acid oxidation. Furthermore, a similar core-shell structure with higher Cu content was fabricated by a simple one-step dealloying process, which also displayed a greatly enhanced catalytic activity towards electroxidation of methanol and formic acid [15]. On the other hand,

it has been observed that the catalytic activity of Pt-Cu alloy catalyst is highly dependent on its composition [16-17], morphology [18] and shape [19]. For instance, the $Pt_{80}Cu_{20}$ nanocube has been identified as the best structure for electrocatalyst by Xu et al. [17] in terms of the electrocatalytic activity and long-term stability.

For the Pt-Cu alloy systems, the enhanced catalytic activity in PEMFC was attributed to the existence of a Pt-skin and its role in the catalytic processes [20]. However, there are many difficulties and challenges in determining the details of the electrochemical process and the enhancement mechanism at the atomic level using the current experimental techniques. As we know, theoretical calculations, especially those based on the density functional theory (DFT) methods, can be very helpful in clarifying the chemical processes on metal surfaces [21-25]. For a large system like the Pt-Cu alloy, many difficulties arise in finding the right geometrical and electronic structures. However, such information is a key to reveal the mechanism of the enhanced catalytic activity.

Due to the size of the system and the number of possible configurations of the low-lying structures, it is extremely difficult to locate the low-lying structures using the existing computing capacity and theoretical methods. For this reason, no theoretical studies about the ground state geometries of large sized Pt-Cu alloy systems have been reported so far. Recently, we have developed an empirical potential model for the Pt-Cu alloys based on the framework of the embedding atom method (EAM), which can and will provide structure optimization of large-sized Pt-Cu alloy systems [26]. Using this potential model, those large Pt-Cu alloy systems can be

studied with more efficiency. To simulate a core-shell structure of Pt-Cu alloy with atomic ratio of Pt:Cu=4:1, it is important to build a suitable model that can balance the cost and precision. In this work, Pt_{108} cluster with 108 atoms was considered due to its enough core and shell positions for Cu doping and an acceptable computational cost. Then 22 Cu atoms randomly replaced 22 Pt atoms to produce Pt-Cu alloy cluster $Pt_{86}Cu_{22}$ with a Pt:Cu ratio of about 4:1. In the present study, the EAM potential model in combination with a Monte Carlo sampling method was used to search for the low-lying structures of $Pt_{86}Cu_{22}$ clusters. The low-lying configurations of these $Pt_{86}Cu_{22}$ clusters were then predicted using the first principles calculations with high accuracy. The structure characteristics of these clusters are in good agreement with the experimental results. In addition, the electronic structures of the selected low-lying configurations were analyzed and used to find the evidences of enhanced catalytic actively of Pt-Cu alloy nanocatalysts.

2. Computation method and details

2.1 Screening Procedure

To generate the isomers of $Pt_{86}Cu_{22}$ cluster, first of all, the cluster of Pt_{108} was selected from face center cubic (fcc) Pt crystal as initial structure. Then, the Pt_{108} cluster was fully optimized by EAM potential with gradient descent algorithm. The optimized Pt_{108} cluster has core-shell geometry with 76 Pt atoms at the surface and 32 Pt atoms inside. Next, 22 Cu atoms were introduced to randomly replace 22 Pt atoms of Pt_{108} cluster, producing the Pt-Cu alloy clusters of $Pt_{86}Cu_{22}$. Specifically, to account for the effect of Cu distribution on the structural stability of $Pt_{86}Cu_{22}$ alloy cluster,

Monte Carlo sampling method together with EAM potential model was employed in the current study. The former is mainly used to randomly generate the isomer structures of $Pt_{86}Cu_{22}$ alloy cluster, and the latter is used to optimize each isomer structure. For example, the Cu atoms have been distributed randomly in a specified range using random number generator. If only the surface Pt atoms were selected to be randomly replaced by Cu atoms, $Pt_{86}Cu_{22}$ clusters with PtCu shell and Pt core will be produced. Similarly, the 22 Cu atoms only randomly replace the Pt atoms in the core part, which will generate the $Pt_{86}Cu_{22}$ isomers with Pt shell and PtCu core. Next, all the isomers of $Pt_{86}Cu_{22}$ clusters were fully optimized by EAM potential with gradient descent algorithm to screen the low-lying structures. Finally, 5 low-lying structures for each doping type were selected according to the energy from the lowest to the high to further predicted by first principles calculations.

2.2 EAM potential of Pt-Cu alloy

Here is a brief description of the EAM potential of Pt-Cu alloy we obtained [26]. In EAM, the total energy of a binary system is written as

$$E_{tot} = \sum_i E_i \tag{1}$$

$$\text{with} \quad E_i = F_\alpha(n_i) + \frac{1}{2}\sum_{\substack{i,j \\ i\neq j}} \Phi_{\alpha\beta}(r_{ij}), \tag{2},$$

where the total potential energy is defined as the sum of potential energy of each atom (E_i). The potential energy E_i includes embedding energy $F_\alpha(n_i)$ and pair potential energy $\frac{1}{2}\sum_{\substack{i,j \\ i\neq j}} \Phi_{\alpha\beta}(r_{ij})$. The indices i and j represent the embedding atom and the neighboring atom, respectively. α and β are element types of the i and j atoms. The specific functions in the model can be expressed as follows:

$$F(n) = F_0[1 - \gamma \ln n]n^{\gamma} + F_1 n \quad (3),$$

$$n_i = \sum_{j \neq i} \rho_{\beta}(r_{ij}) \quad (4),$$

$$\rho_{\beta}(r) = \Psi\left(\frac{r - r_c}{h}\right) \frac{1 + \alpha_1 \cos(\alpha r + \varphi_1)}{r^{\beta}} \quad (5),$$

$$\Phi(r) = \Psi\left(\frac{r - r_c}{h}\right)\left[\frac{C_1}{r^{\eta_1}} + \frac{C_2}{r^{\eta_2}}\cos(kr + \varphi_2)\right] \quad (6),$$

$$\Psi(\mathrm{x}) = \frac{x^4}{1 + x^4} \quad (7).$$

F_0, γ, F_1, h, α_1, α,φ_1, β, C_1, η_1, C_2, η_2, k, φ_2 are parameters determined by fitting the model, and r_c is cutoff distance of the EAM potential. The function of $\rho_{\beta}(r_{ij})$ is an empirical quantity, representing electron density transferred to position of atom *i* from atom *j*. Ψ(x) is a cutoff function which ensures that the functions smoothly go to zero near the cutoff distance.

2.3 First Principles Calculations

In this work, all the first principles calculations were carried out by the Vienna *Ab-initio* Simulation Package (VASP) [27-28] based on the DFT with projector-augmented wave (PAW) approach [29-30]. The generalized gradient approximation (GGA) in the form of PW91 function was used for the exchange-correlation interaction [31]. Pt $5d^9 6s^1$ and Cu $3d^{10} 4s^1$ were treated as valence electrons, and the cut-off energy of 400 eV was set for the plane wave basis. In the geometry optimization, the maximum of Hellman-Feynman force on each atom was chosen to be 0.01 eV/Å, and the electronic iterations convergence was set to be 1×10^{-5} eV. To prevent the interaction between images of $Pt_{86}Cu_{22}$, a vacuum region of 15 Å was created along the *x*, *y*, and *z* direction, respectively. The dipolar corrections in all directions were also considered in all the calculations.

3. Results and discussions

3.1 Structure and Stability of $Pt_{86}Cu_{22}$ Clusters

Using the computational scheme described in Sect. 2, we cut out a cluster of 108 Pt atoms from fcc Pt crystalline and then fully optimized the structure by EAM potential. As illustrated in Fig.1, there are 76 Pt atoms on the surface of Pt_{108} cluster, while 32 Pt atoms located inside of the Pt_{108} cluster, which makes Pt_{108} cluster a spherical core-shell geometry with a diameter of 14 Å. To generate a Pt-Cu alloy cluster with an atomic ratio of 4:1, 22 Pt atoms in the Pt_{108} cluster were randomly substituted by 22 Cu atoms. In order to investigate the distribution features of Cu atoms in Pt_{108} cluster, three doping types of Pt-Cu alloy cluster were considered. Type I is only 22 core Pt atoms were substituted, noted as doping-core, that is Pt@PtCu; type II is both surface and core Pt atoms were randomly selected to be replaced, noted as doping-normal, that is PtCu@PtCu; and type III is only the surface 22 Pt atoms were randomly substituted, noted as doping-shell, that is PtCu@Pt. Three doping types are illustrated in Fig. 2.

For each doping type, 10^5 isomers of $Pt_{86}Cu_{22}$ cluster were generated randomly and optimized by EAM potential with gradient descent algorithm. To evaluate the relative stability of isomers, the cohesive energy of each $Pt_{86}Cu_{22}$ alloy cluster and the average cohesive energy of 10^5 isomers for each doping type were computed by the formulas

$$E_{\text{cohesive}} = E_{cluster} - N_{Pt}E_{Pt_{isolate}} - N_{Cu}E_{Cu_{isolate}} \quad (8)$$

and

$$E_{\text{avecohesive}} = (E_{cluster} - N_{Pt}E_{Pt_{isolate}} - N_{Cu}E_{Cu_{isolate}})/n \quad (9),$$

where $E_{cluster}$ is the total energy of each $Pt_{86}Cu_{22}$ alloy cluster, N_{Pt} and N_{Cu} are the number of Pt atom and Cu atom in $Pt_{86}Cu_{22}$ alloy cluster, that is 86 and 22. $E_{Pt_{isolate}}$ and $E_{Cu_{isolate}}$ are the energy of isolate Pt atom and Cu atom, respectively. n is the number of isomers, that is 10^5 in Table 1 and 5 in Table 2. The average cohesive energies of 10^5 isomers for each doping type from EAM potential were listed in Table 1, and the cohesive energies of each selected low-lying structure and the average cohesive energies for each doping type from DFT level were summarized in Table 2. Obviously, from Table 1, the average cohesive energy is in order of doping-core < doping-normal < doping-shell, indicating that the stability of each doping type is in order of doping-shell < doping-normal < doping-core. The result indicates that the Cu atoms prefer to be located in the core region. To further verify this, five low-lying isomers for each doping type were selected and fully relaxed using the first principles calculations. Clearly, from Table 2, the average cohesive energy of three doping types follows the same order: doping-core < doping-normal < doping-shell, which is consistent with the result from the EAM calculations. So, we fully believe that the optimal structure of Pt-Cu alloy nanocluster is core-shell geometry with Pt shell and PtCu alloy core. This result is in good agreement with the observation from experiment [14], where a novel nanoporous Pt-Cu bimetallic catalyst with a Pt skin and a PtCu core had been successfully fabricated by using electrochemically dealloying method. In addition, it indicates that the combination of EAM and Monte Carlo method is of great advantage in treating such large sized Pt-Cu alloy systems and can give reliable results.

Table1 Average cohesive energy (in eV) of $Pt_{86}Cu_{22}$ isomers obtained by EAM potential for three doping types: doping-core, doping-normal, and doping-shell.

doping type	isomer number	Average cohesive energy
doping-core	1×10^5	-483.866
doping-normal	1×10^5	-483.045
doping-shell	1×10^5	-477.324

Table 2 Cohesive energy (in eV) of each selected low-lying structure and average cohesive energies for each doping type, obtained from first principles calculations.

	doping-core	doping-normal	doping-shell
Low-1	-488.963	-484.690	-477.997
Low-2	-486.407	-484.362	-479.425
Low-3	-487.003	-485.751	-478.276
Low-4	-486.131	-484.661	-479.758
Low-5	-488.041	-484.722	-479.641
Average	-487.309	-484.837	-479.019

To further investigate how the distance of doped Cu atoms to the center of Pt-Cu alloy cluster affects the stability of Pt-Cu alloy system, one Cu atom doping, the simplest case, was treated to show the Cu position effect. Here, 108 isomers were fully optimized by EAM potential, and the total energy of each isomer versus the distance of Cu atom to the center of cluster was shown in Fig.3. As seen from Fig. 3,

with the distance increasing, the total energy of $Pt_{107}Cu$ cluster decreases first, and reaches the minimum near the surface. Then, it increases as the distance increases, and eventually converges to the surface distance. The trend of total energy versus distance indicates that the Cu atom doping at the subsurface is more stable than that at the surface or center positions. In addition, Fig.3 also shows three typical structures of one Cu atom doping with the different distance to the center of cluster, obtained from screening by EAM potential. The total energies along with the R (R represents the distance of Cu atom to the center of $Pt_{107}Cu$ cluster) again suggest that the Cu atoms prefer to be located at the subsurface instead of surface and center positions.

Furthermore, to find out whether the doped Cu atoms are assembled or dispersed in the Pt-Cu alloy systems, the Cu-Cu pair distribution functions were examined. From the above calculations, it is found that the total energy of Pt-Cu alloy system strongly depends on the doping position of Cu atoms. Thus, to eliminate the contribution of different positions of Cu atoms to the total energy, we constructed a very large system of cubic nanocrystal (NC) contains 1372 Pt atoms, then 27 Cu atoms randomly replaced 27 Pt atoms which are more than 6 Å away from the surface (equal to the cutoff distance r_c of the EAM potential). In this model, all doped Cu atoms are equivalent, which can avoid the effects of a preferred position. Such a large model ensures that the energy differences among the isomers only arise from the different Cu interatomic distances. In the present work, 10^5 isomers of $Pt_{1345}Cu_{27}$ NC were calculated with adequate accuracy by EAM potential. The optimized structure of $Pt_{1345}Cu_{27}$ NC with the lowest and highest energy is shown in Fig.4a and 4b,

respectively. Clearly, the distribution of Cu atoms is dispersed in the lowest-energy NC and concentrated in the highest-energy NC. Next, we have selected 100 low energy structures and 100 high energy structures from 10^5 isomers of $Pt_{1345}Cu_{27}$ NC, and calculated their average Cu-Cu radial pair distribution functions, as shown in Fig.5. Apparently, the content of the Cu-Cu pairs in low energy structures smaller than those in the high energy structures, indicating that doped Cu atoms in the doped materials prefer a dispersed state rather than a congregated arrangement.

3.2 Electronic Structure Analysis

The catalytic properties are in principle determined by the electronic structure, so it is of significant importance to conduct the electronic structure calculations and analyses. In order to understand the nature of enhanced catalytic activity of Pt-Cu alloy as compared with pure Pt system, the projected electron densities of states of surface Pt atoms of Pt-Cu alloy cluster and pure Pt cluster were examined. Typically, the surface Pt atom nearest to the subsurface Cu atom (Pt_{sur}, represented by a small blue ball in Fig.6) was selected as an example to show the doping effect. For simplicity, one Cu atom doping case was considered, as shown in Fig.6. For comparison, the Pt atom in a pure Pt_{108} cluster located at the same position was also analysed. The projected density of states (PDOS) of the Pt_{sur} in $Pt_{107}Cu$ and Pt_{108} was also shown in Fig.6, respectively. From Fig.6 (a), it is observed that the total density of states (TDOS) of Pt_{sur} atom in $Pt_{107}Cu$ and Pt_{108} mainly comes from the *d*-orbitals, the contribution of the *s*-orbital and the *p*-orbital is almost zero. Furthermore, a new peak appears near the Fermi level in the TDOS and the *d*-orbital of Pt_{sur} in $Pt_{107}Cu$

cluster, meaning that Pt alloying with Cu enriches the electronic states of the surface Pt atom in the vicinity of the Fermi level. Thus the electronic structure of surface Pt is tuned after alloying with Cu, which may lead to the enhancement of the electrocatalytic activity of Pt-Cu alloy for the ORR.

In addition, Fig.6 (b) clearly shows that *d* orbitals of the surface Pt atom have been changed from unoccupied states in pure Pt_{108} cluster to occupied states in Cu-doped $Pt_{107}Cu$ cluster. This change means that *d* orbitals of the Pt_{sur} atom may accept electrons after alloying with Cu. This should facilitate the electron transfer from the Pt surface to oxygen in the ORR process and enhance the reduction of oxygen in PEMFE. On the other hand, the analysis of Bader charge indicates that there exists a significant electron transfer from Cu to Pt in $Pt_{107}Cu$ cluster. The calculated Bader charge of the Cu atom is 10.56 electrons, showing a charge transfer of 0.44 e from Cu to Pt. Combining with the analysis of aforementioned PDOS, we conclude that the charge mainly transfers to the *d* orbitals of Pt_{sur} atom.

For low-lying structures of $Pt_{86}Cu_{22}$ clusters, the transferred Bader charge from Cu atom to Pt atom is in the range of 0.3-0.4e. The electron density of states of surface Pt atoms of $Pt_{86}Cu_{22}$ alloy clusters also exhibits the abundant electron states near the Fermi level compared with those of pure Pt_{108} cluster. The comparative results of electronic structure analysis for $Pt_{107}Cu$ and $Pt_{86}Cu_{22}$ clusters agree well with those from small sized Pt_nCu alloy clusters [32].

4. Conclusions

In this paper, the low-lying structures of $Pt_{86}Cu_{22}$ cluster were screened by using the

EAM potential combined with the Monte Carlo sampling method. From the cohesive energy of three doping types (doping-core, doping-normal, and doping-shell) of $Pt_{86}Cu_{22}$ cluster, we found that Pt@PtCu core-shell structures with Pt shell and PtCu alloy core are more stable than the other ones, which is in good agreement with the observation from the experiments. Furthermore, the optimal doping position of Cu atom in Pt-Cu alloy clusters is at subsurface instead of surface or center positions, and the doped Cu atoms prefer to disperse rather than to congregate in the Pt-Cu alloy. Finally, the comparative analysis of the PDOS of surface Pt atom in Pt-Cu alloy cluster and pure Pt cluster indicates that Cu doping can obviously enrich the electronic states of surface Pt atoms near the Fermi level. The Bader charge analysis also shows that there exists a charge transfer from Cu to Pt in Pt-Cu alloy clusters. These findings are expected to help in understanding of the mechanism of enhanced catalytic activity for Pt-Cu alloy catalysts.

Acknowledgments

The authors thank the National Science Foundation of China (Grant No. 11404149, 11764019, 11664013, 11664012, and 11564016) for major financial support of the current work. Partial support to B. Xu from the Science and Technology Department of Jiangxi Province (Grant No. 20152ACB21014) is also appreciated. The partial computations were performed on TianHe-1 (A) at the National Supercomputer Center in Tianjin.

References

[1] Y. Wang, K. S. Chen, J. Mishler, S. C. Cho, X. C. Adroher, Appl. Energy 88 (2011) 981.

[2] H. Yang, L. Dai, D. Xu, J. Fang, S. Zou, Electrochim. Acta. 55 (2010) 8000.

[3] R. Mu, Q. Fu, H. Xu, H. Zhang, Y. Huang, Z. Jiang, S. Zhang, D. Tan, X. Bao, J. Am. Chem. Soc. 133 **(**2011) 1978.

[4] Z. Yu, J. Zhang, Z. Liu, J. Ziegelbauer, H. Xin, I. Dutta, D. Muller, F. Wagner, J. Phys. Chem. C 116 (2012) 19877.

[5] H. Yang, J. Zhang, K. Sun, S. Zou, J. Fang, Angew. Chem. 122 (2010) 7000.

[6] D. Chung, S. Jun, G. Yoon, J. Am. Chem. Soc. 137 (2015**)** 15478.

[7] H. Zhang, M. Jin, Y. Xia, Chem. Soc. Rev. 41 (2012**)** 8035.

[8] A. X. Yin, X. Q. Min, W. Zhu, W. C. Liu, Y. W. Zhang, C. H. Yan, Chem. Eur. J. 18 (2012) 777.

[9] D. Wang, P. Zhao & Y. Li, Scientific Reports 1:37 (2011) DOI: 10.1038/srep00037.

[10] Z. Xu, H. Zhang, S. Liu, B. Zhang, H. Zhong, D. Su, Int. J. Hydrogen Energy 37 (2012) 17978.

[11] O. Sorsa, H. Romar, U. Lassi, T. Kallio, Electrochim. Acta. 230 (2017) 49.

[12] G. Caballero-Manrique, I. Nadeem, E. Brillas, F. Centellas, J. Garrido, R. Rodríguez, P. Cabot, Catalysts 6 (2016) 125.

[13] Z. Zhang, Z. Luo, B. Chen, C. Wei, J. Zhao, J. Chen, X. Zhang, Z. Lai, Z. Fan, C. Tan, M. Zhao, Q. Lu, B. Li, Y. Zong, C. Yan, G. Wang, Z. Xu, H. Zhang, Adv. Mater. 28 (2016) 8712.

[14] X. Ge, L. Chen, J. Kang, T. Fujita, A. Hirata, W. Zhang, J. Jiang, M. Chen, Adv. Funct. Mater. 23 (2013) 4156.

[15] H. Qiu, H. Xu, X. Li, J. Wang, Y. Wang, J. Mater. Chem. A 3 (2015) 7939.

[16] Y. Jiang, Y. Jia, J. Zhang, L. Zhang, H. Huang, Z. Xie, L. Zheng, Chem. Eur. J. 19 (2013) 3119.

[17] D. Xu, S. Bliznakov, Z. Liu, J. Fang, N. Dimitrov, Angew. Chem. 122 (2010) 1304.

[18] X. Huang, Y. Chen, E. Zhu, Y. Xu, X. Duan, Y. Huang, J. Mater. Chem. A 1 (2013) 14449.

[19] L. Bromberg, M. Fayette, B. Martens, Z. Luo, Y. Wang, D. Xu, J. Zhang, J. Fang, N. Dimitrov, Electrocatalysis 4 (2013) 24.

[20] Y. Xu, A. Ruban, M. Mavrikakis, J. Am. Chem. Soc. 126 (2004) 4717.

[21] J. Mejía-López, G. García, A. H. Romero, J. Chem. Phys. 131 (2009) 044701.

[22] A. S. Chaves, M. J. Piotrowski, D. Guedes-Sobrinho, J. L. F. Da Silva, J. Phys. Chem. A 119 (2015) 11565.

[23] V. I. Avdeev, V. I. Kovalchuk, G. M. Zhidomirov, J. L.d'Itri, Surface Science 583 (2005) 46.

[24] D. Guedes-Sobrinho, R. K. Nomiyama, A. S. Chaves, M. J. Piotrowski, J. L. F. Da Silva, J. Phys. Chem. C 119 (2015) 15669.

[25] A. S. Chaves, G. G. Rondina, M. J. Piotrowski, J. L. F. Da Silva, Comp. Mat. Sci. 98 (2015) 278.

[26] H. Mu, B. Xu, C. Ouyang, X. Lei, J. Alloys Compd. 696 (2017) 470.

[27] G. Kresse, J. Hafner, Phys. Rev. B 47 (1993) 558.

[28] G, Kresse, J. Furthmüller, Phys. Rev. B 54 (1996) 11169.

[29] P. E. Blöchl, Phys. Rev. B 50 (1994) 17953.

[30] G. Kresse, D. Joubert, Phys. Rev. B 59 (1999) 1758.

[31] Y. Wang, J. P. Perdew, Phys. Rev. B 44 (1991) 13298.

[32] X. L. Lei, M. S. Wu, G. Liu, B. Xu, and C. Y. Ouyang, J. Phys. Chem. A 117 (2013) 8293.

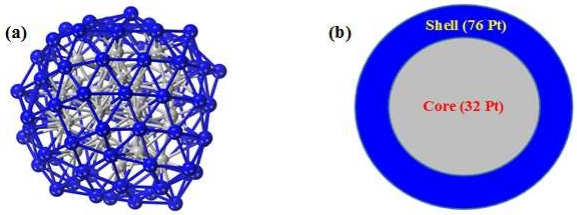

Fig. 1(a) is the optimized structure of Pt_{108} cluster; (b) is schematic diagram of illustration of core-shell structure in Pt_{108}. Blue and grey balls present shell and core Pt atoms, respectively.

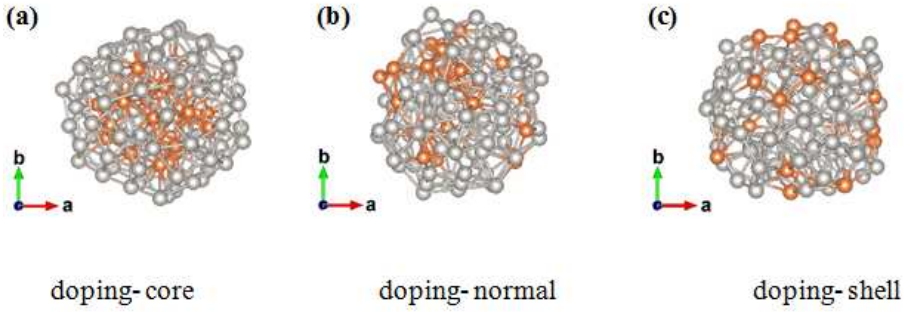

Fig.2 Three doping types of Pt-Cu alloy clusters $Pt_{86}Cu_{22}$.

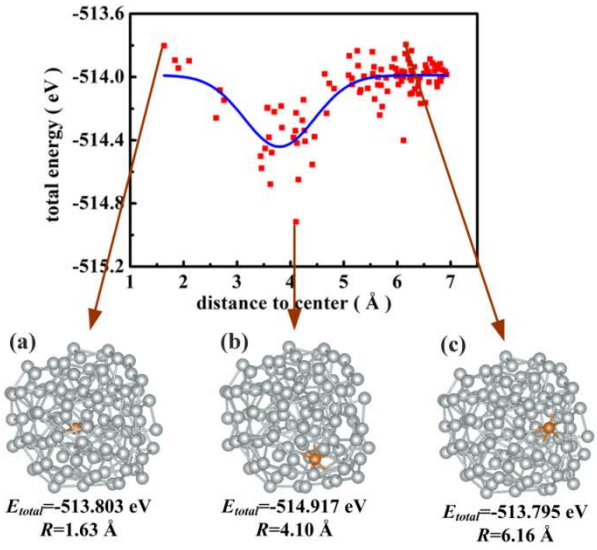

Fig. 3 Total energy *versus* distance of Cu atom to the center of $Pt_{107}Cu$ cluster, and three typical structures of $Pt_{107}Cu$ cluster from screening by EAM potential: (a) Cu atom located in the center of $Pt_{107}Cu$; (b) Cu atom located at the subsurface of $Pt_{107}Cu$; (c) Cu atom located at the surface of $Pt_{107}Cu$. *R* denotes the distance of Cu atom to the center of $Pt_{107}Cu$ cluster.

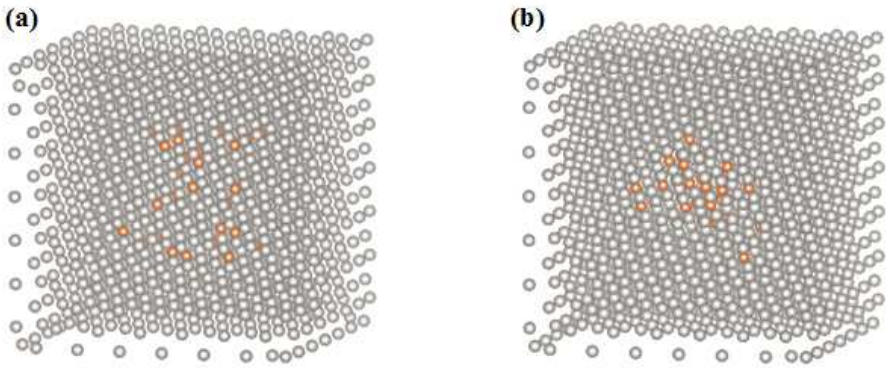

Fig.4 Optimized structures of the lowest-energy isomer (a) and the highest-energy isomer (b) of $Pt_{1345}Cu_{27}$ Cubic Nanocrystal from Embedding Atom Method potential screening.

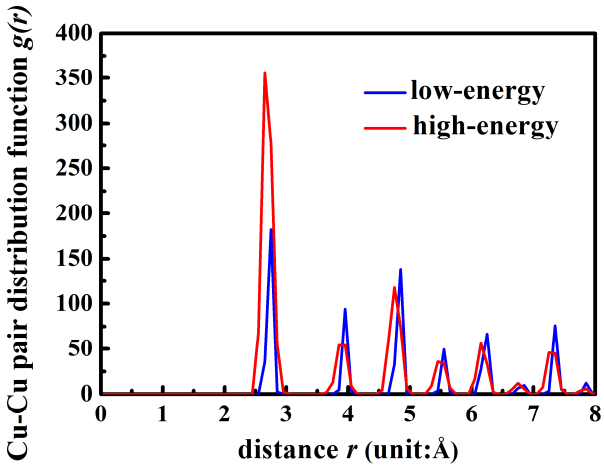

Fig.5 Average Cu-Cu pair distribution functions for 100 low-energy isomers of the $Pt_{1345}Cu_{27}$NC and 100 high-energy isomers of the $Pt_{1345}Cu_{27}$ Cubic Nanocrystal, respectively.

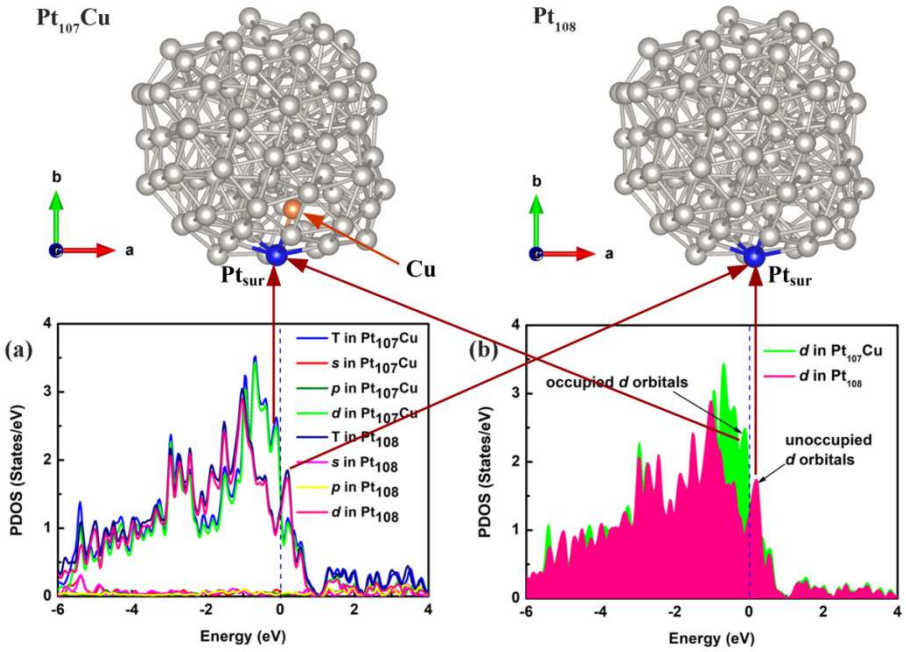

Fig.6 Structures of single Cu atom doped $Pt_{107}Cu$ cluster and pure Pt_{108} cluster, and PDOS of the surface Pt atom (Pt_{sur}) in Cu doped cluster $Pt_{107}Cu$ and pure Pt cluster Pt_{108}. The blue ball and orange ball represent Pt_{sur} atom and Cu atom, respectively.

1. The low-lying structures of $Pt_{86}Cu_{22}$ have been confirmed by the EMD.
2. The low-lying structures of $Pt_{86}Cu_{22}$ show a Pt@PtCu core-shell structure.
3. The Cu atoms prefer positions at subsurface instead of surface of $Pt_{86}Cu_{22}$.
4. The Cu atoms are dispersed in Pt-Cu alloy.
5. The PDOS show that Cu enriches the electronic states of surface Pt.